Research Article

Design and analysis of photonic crystal fiber-based plasmonic microbiosensor: an external sensing scheme

Md. Mahabubur Rahman[1] · Md. Masud Rana[2] · M. S. Anower[2] · M. Saifur Rahman[2] · Alok Kumar Paul[2]

Abstract

In this paper, a highly sensitive gold-coated plasmonic microbiosensor, based on photonic crystal fiber (PCF), is proposed and numerically analyzed. To minimize the fabrication challenge and to aid the real-time detection capability of the sensor, the external sensing approach is utilized here. To introduce birefringence property, two rings with some missing air holes are used. Both the wavelength interrogations, as well as the amplitude interrogation method, have been used to determine the sensitivity of the modeled sensor. To demonstrate better performance, different structural parameters, e.g., the thickness of gold layer, pitch, and the diameter of air holes of the PCF, have been varied and investigated. The sensor shows a maximum possible wavelength sensitivity of 10,000 nm/RIU and a maximum possible amplitude sensitivity of 1250 RIU^{-1} with a sensor wavelength resolution of 1.0×10^{-5} RIU. The proposed sensor exhibits an admirable figure of merit (FOM) of the highest value of 260.86 RIU^{-1} with an excellent linearity property of resonance wavelength in terms of analyte refractive indices. The designed sensor reveals promise for sensing and detecting different biological and biochemical liquid analytes of refractive index (RI) ranging from 1.33 to 1.39 with having enhanced performance.

1 Introduction

Surface plasmon resonance (SPR) is a process of generation and propagation of transverse magnetically polarized electromagnetic waves restricted to a narrow range on metal–dielectric interface due to the incidence of the light wave at the interface. The light wave energy coupling to the interface causes a combined oscillation of electrons when the oscillation frequency of electrons and frequency of light wave matches [1, 2]. In this special condition, resonance occurs, and the energy of the light wave is converted into free electron's combined oscillation energy [1–3].

In the last few decades, researchers have found intense interest in SPR-based sensors as they have been used widely in myriad fields of everyday life due to their high sensitivity characteristics, fast response, level-free, and real-time detection capability of multiple biological and biochemical samples [4–6]. The theoretical reflection about SPR has been established by Ritchie et al. [7] in the 1957s. SPR theory of Ritchie was experimentally proven by Powel et al. in 1983 and familiarized practically based on prism coupler that is limited to use in remote sensing application. It is also bulky in size owing to different types of mechanical and optical portions. Based on optical fiber with a gold coating used as plasmonic material, SPR sensor was suggested by R.C. Jorgenson et al. in 1993, which overcame the limitations of prism-based SPR sensors [2, 8]. Another window has been opened while photonic crystal fiber (PCF) sensors are proposed, which removes the

✉ Md. Mahabubur Rahman, mahabubkanon@gmail.com | [1]Department of Electrical and Computer Engineering, Rajshahi University of Engineering and Technology, Rajshahi 6204, Bangladesh. [2]Department of Electrical and Electronic Engineering, Rajshahi University of Engineering and Technology, Rajshahi 6204, Bangladesh.

margins of conventional fiber, e.g., limited design parameters [9]. Taking the advantages of PCF such as flexible structure, highly sensitive and controllable birefringence characteristics, high confinement, lower electromagnetic interference, single mode propagation, etc. [10]., nowadays, researchers have paid a keen interest to design distinct structures and to improve the performance characteristics of SPR-based PCF sensor as they can be applied to diverse fields, e.g., medical diagnostics, bio-sensing [11], gas detection, water testing, glucose monitoring, bio-imaging [6],virus detection [11], drug testing [12], biotechnology, chemical sensing [13], and so on. Usually, silver, gold, aluminum, and copper are used as plasmonic material, and most of the PCF-based SPR sensor used gold or silver in recent years [6, 8]. But, silver used as a plasmonic material introduces the oxidation problem which reduces the performance and detection accuracy of the sensor. On the contrary, gold provides more stability while coming in contact with chemicals. In this work, we use gold as a plasmonic material on the outer surface of PCF which removes the fabrication complexity as compared to an internally metal film-coated sensor [14, 15].

Nowadays, researchers are trying to develop a distinct structure for enhancing the performance of the sensor. In this regard, Xudong et al. [16] proposed an SPR PCF biosensor that shows amplitude sensitivity up to maximum value of 641 RIU^{-1} and wavelength sensitivity of 11,000 nm/RIU. This sensor can detect the analyte RI ranging from 1.350 to 1.395 with a sensor resolution of 9.09×10^{-5} RIU. Similarly, Sujan et al. [17] reported a gold-coated PCF biosensor based on SPR, where the background material of the sensor is considered as fused silica. Their proposed sensor is capable of detecting analyte RI ranging from 1.34 to 1.37 with a sensor resolution of 1.11×10^{-5} RIU. The maximum amplitude sensitivity and wavelength sensitivity of the sensor is reported 318 RIU^{-1} and 9000 nm/RIU, respectively. In the same way, Rifat et al. [18] also proposed a gold-coated PCF biosensor based on the external sensing approach. Their sensor can operate on analyte RI ranging from 1.33 to 1.37 with a maximum amplitude sensitivity and wavelength sensitivity of 478 RIU^{-1} and 4000 nm/RIU, respectively. The sensor provides maximum resolution of 2.5×10^{-5} RIU. Also, Zhou et al. [19] recommended a ring-shaped externally gold-coated PCF sensor for practical sensing approach. The proposed sensor shows a maximum wavelength sensitivity and amplitude sensitivity of 6900 nm/RIU and 132 RIU^{-1} for analyte RI ranging from 1.33 to 1.41. Likewise, Hasan et al. [20] proposed a plasmonic RI sensor based on gold and niobium nanofilm with a thin layer of aluminum oxide (Al_2O_3) film on the surface of niobium film. Their reported values of the maximum wavelength sensitivity and amplitude sensitivity are of 8000 nm/RIU and 1560 RIU^{-1}, respectively. Their proposed

sensor shows a maximum resolution of 8.64×10^{-5} RIU for the detection range of analyte RI, ranging from 1.36 to 1.40. Paul et al. [21] also reported a dual-core structure of SPR biosensor with a maximum amplitude sensitivity and wavelength sensitivity of 636.5 RIU^{-1} and 11,500 nm/RIU, respectively. The detection range of analyte RI of 1.33 to1.41 with a sensor resolution of 8.7×10^{-6} RIU. Very recently, Akter and Razzak [22] proposed an open channel-based PCF biosensor based on SPR for using in visible to near-infrared region. It has been reported that the highest value of wavelength and amplitude sensitivity of the sensor is 5000 nm/RIU and 396 RIU^{-1}, respectively. The sensor can detect the analyte of RI, ranging from 1.33 to 1.38, with a maximum sensor resolution of 2.0×10^{-5} RIU.

In this paper, a PCF microbiosensor based on SPR technology is proposed where two rings with some missing holes are used to introduce birefringence property that confirms superior performance such as better amplitude sensitivity, wavelength sensitivity as well as sensor resolution. To obtain better performance and to assess the effect of variation of different structural parameters on the performance of the sensor, the thickness of gold layer, pitch, and the diameter of air holes, etc. are tuned and optimized.

2 Geometrical structure and Design consideration

The cross-sectional view of the proposed sensor is illustrated in Fig. 1a. Two air hole rings are considered in designing the sensor of having an air hole to air hole distance of $\Lambda = 1.5$ μm. The air holes of the inner ring are of the diameter of $d_1 = 0.2 \times \Lambda$ μm where four air holes are missing to create a channel for effective interaction of the evanescent field to SPP mode at the metal–dielectric interface. The outer ring consists of air holes of two different diameters where smaller air holes are of a diameter of $d_2 = 0.5 \times d_1$ μm and larger air holes are of the diameter of d_1. The air holes of the outer ring facilitate the light with better confinement in the core region. The smaller air hole of the outer ring is placed upon the missing air holes of the inner ring. There are also three air holes inside the core except for these two rings. One of them, having a diameter of $d_3 = 0.3 \times \Lambda$ μm, is placed at the center and the other two with diameter d_1 surrounds the right and left of the centered one. These air holes combined with smaller air holes of the outer ring are used for introducing the birefringence effect. A thin layer of gold is considered as plasmonic material around the fiber. The sample, called analyte to be detected, having thickness 1.2 μm is positioned at immediate to the plasmonic material of a thickness of $t_g = 35$ nm, which is followed by 1.25 μm perfectly matched layer (PML).
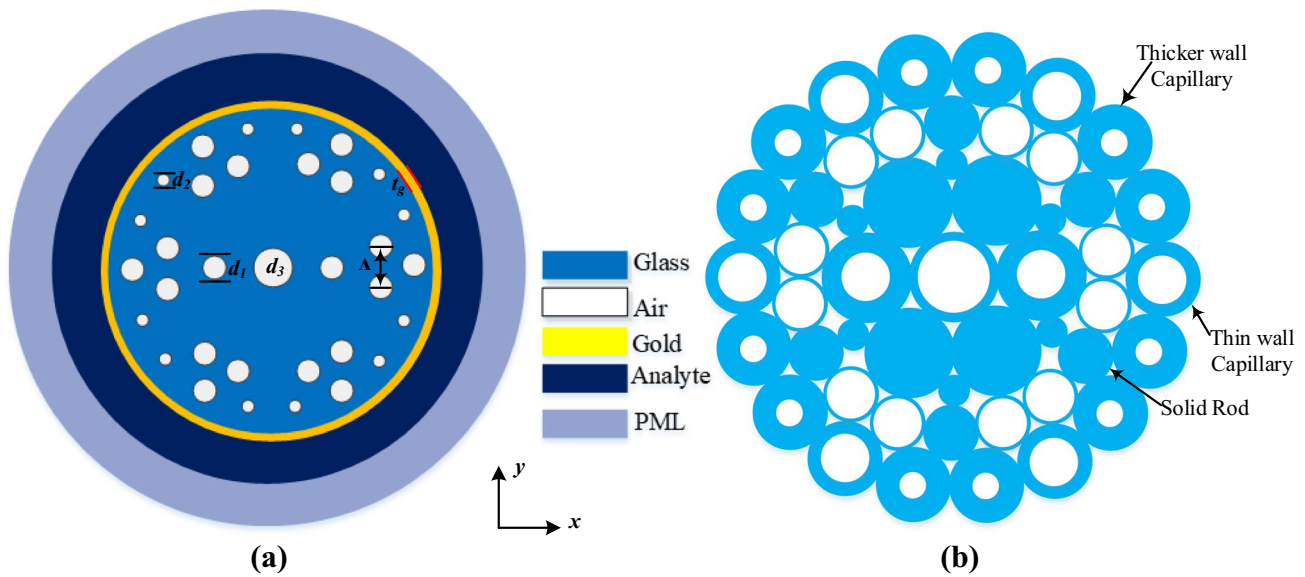
Fig. 1 Cross-sectional view of **a** the proposed SPR biosensor and, **b** the stacked preform structure, in x–y plane

PCF fabrication process requires two main steps: making a fiber preform and drawing it using a high temperature furnace in a standard fiber drawing tower. After preparation of fiber preform, silica rods, and capillaries are stacked together called stacked preform and drawn down it [21]. Guiding cores are created by inserting deliberate defects in the structure, for instance, by replacing a capillary with a solid rod or leaving many capillaries out altogether [23–25]. Moreover, thin and thick capillaries are used to create big and small air holes, respectively, as shown in Fig. 1b. Deposition of gold layer on the PCF is an important issue that requires high temperature in some deposition techniques. Moreover, electron beam evaporation technique which operates at high pressure and low temperature, can be utilized to deposit the gold layer efficiently [26].

In this design, the refractive index of background material is considered as silica glass. The refractive index of silica is calculated from the Sellimeiers equation [27]. Here, gold is used as plasmonic material, and the refractive index of the material is calculated from the Drude–Lorentz model [28]-based wavelength-dependent equation as follows.

$$n_{au}^2(\lambda) - 1 = \frac{\lambda^2 \lambda_c}{\lambda_p^2 (\lambda_c + i\lambda)} \tag{1}$$

where λ_p and λ_c are plasma and collision wavelength, respectively. The values of λ_p and λ_c for gold are 0.16826 μm and 8.9342 μm, respectively [28].

3 Results and analysis

SPR sensors operate based on the principle of interaction of evanescent fields with the analytes. In the case of PCF sensors, the arrangement is made in such a way that light can escape from core to cladding. This leakage light excites the electrons of the metal–dielectric interface, causing surface plasmon. At a particular wavelength of light, called resonant wavelength, maximum energy is absorbed by the electrons at the interface. This particular condition happens when the effective refractive index of core guided mode matches perfectly with the SPP mode. In the case of PCF-based sensors, it is often found that the sensors are capable working in a dual-polarized (both for the x-component and y-component of light) mode with nearly same output characteristics and sometimes are not. This phenomena arises because of the implementation of the birefringence property that is related to the PCF geometric structure [2, 3].

Figures 2 and 3 reflect the dispersion profile of the raised structure where Fig. 2 indicates the variation of optical field scattering of fundamental core guided mode and spp mode both for both x- and y-component of light. The change in refractive indices occur due to the birefringence property of the structure raised here. In Fig. 3, loss spectrum is directed by a solid green line, whereas the dotted black and red lines direct the real part of fundamental core guided mode and SPP mode, separately. It is perceived that resonance occurs at the
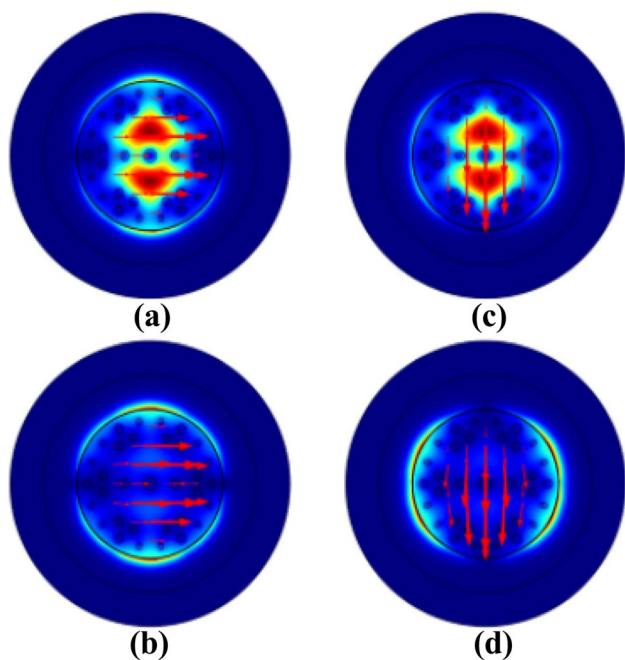
Fig. 2 Optical field scattering of the proposed sensor for *x*-component of light for **a** core guided mode, **b** spp mode, and *y*-component of light for **c** core guided mode **d** spp mode
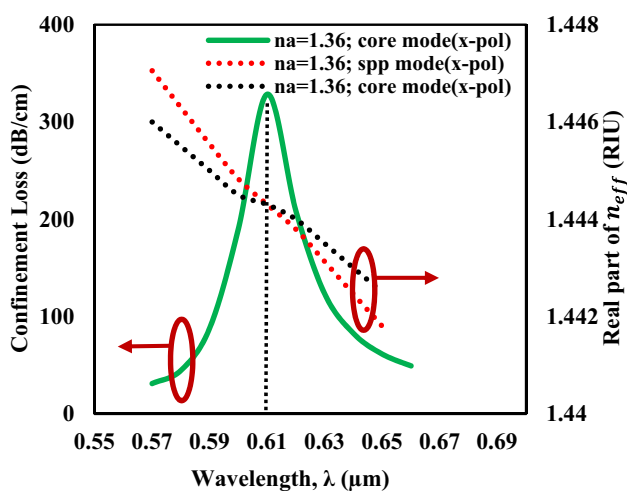

Fig. 3 Dispersion profile of the sensor for *x*-component of light with analyte RI of 1.36 screening loss spectrum (solid green line), fundamental core guided mode (dotted black line), and spp mode (dotted red line)

wavelength of 610 nm where the real part of effective refractive index (n_{eff}) of core guided mode equals the SPP mode. At this condition, maximum confinement loss occurs for a particular analyte RI. The confinement loss is calculated using the following equation [29].

$$\alpha_{loss}(dB/cm) \approx 8.686 \times \frac{2\pi}{\lambda} \cdot Im(n_{eff}) \times 10^4 \qquad (2)$$

where n_{eff} represents the effective refractive index and λ is the wavelength of incident light in micron. The finite element method (FEM)-based COMSOL multiphysics software is used for computational analysis of the proposed structure. In the case of analysis, a physics-controlled mode of meshing is considered and a normal mode of mesh size is selected that creates 181,119 number of triangular meshing subdivisions of the whole structure for computation. The imaginary part of n_{eff} is determined by COMSOL multiphysics software which is used for further calculation of different performance parameters of the sensor.

Before analyzing different performance measuring parameters of the proposed sensor the thickness of the gold layer is optimized considering the amplitude interrogation method. The effect of variation of the thickness of the gold layer is illustrated in Fig. 4a–d. Then, the thickness of the gold layer is varied from 30 to 45 nm with an interval of 5 nm and confinement loss for the proposed sensor is calculated both for both *x*- and *y*-component of light. Then, amplitude sensitivity of the sensor is determined using the following equation [30].

$$S_A(1/RIU) = -\frac{\partial\alpha(\lambda, n_a)/\partial n_a}{\alpha(\lambda, n_a)} \qquad (3)$$

Here $\alpha(\lambda, n_a)$ denotes propagation loss of the sensor at analyte RI of n_a which is also a function of wavelength and $\partial\alpha(\lambda, n_a)$ is the difference between two loss curves for two consecutive analyte RI at a particular wavelength. The solid line in the spectra indicates the loss for an analyte RI of 1.37 and the dotted line is for 1.38. It is evident that the amplitude sensitivity of the sensor decreases with the escalation of gold thickness.

It is observed that the deviation of amplitude sensitivity for the gold thickness of 30 nm and 35 nm is very small in the case of *y*-component of light and maximum sensitivity is attained here. Hence, the thickness of the gold is selected 35 nm to minimize the fabrication challenge as a thinner layer is difficult to formulate. The further performance analysis of the proposed sensor is performed considering 35 nm thickness of gold.

3.1 Wavelength sensitivity

The sensitivity of the proposed sensor is also measured using phase detection or wavelength interrogation method. It is investigated by changing the analyte refractive indices from 1.33 to 1.39. The wavelength interrogation method with the following equation is applied for determining the wavelength sensitivity of the sensor [28].
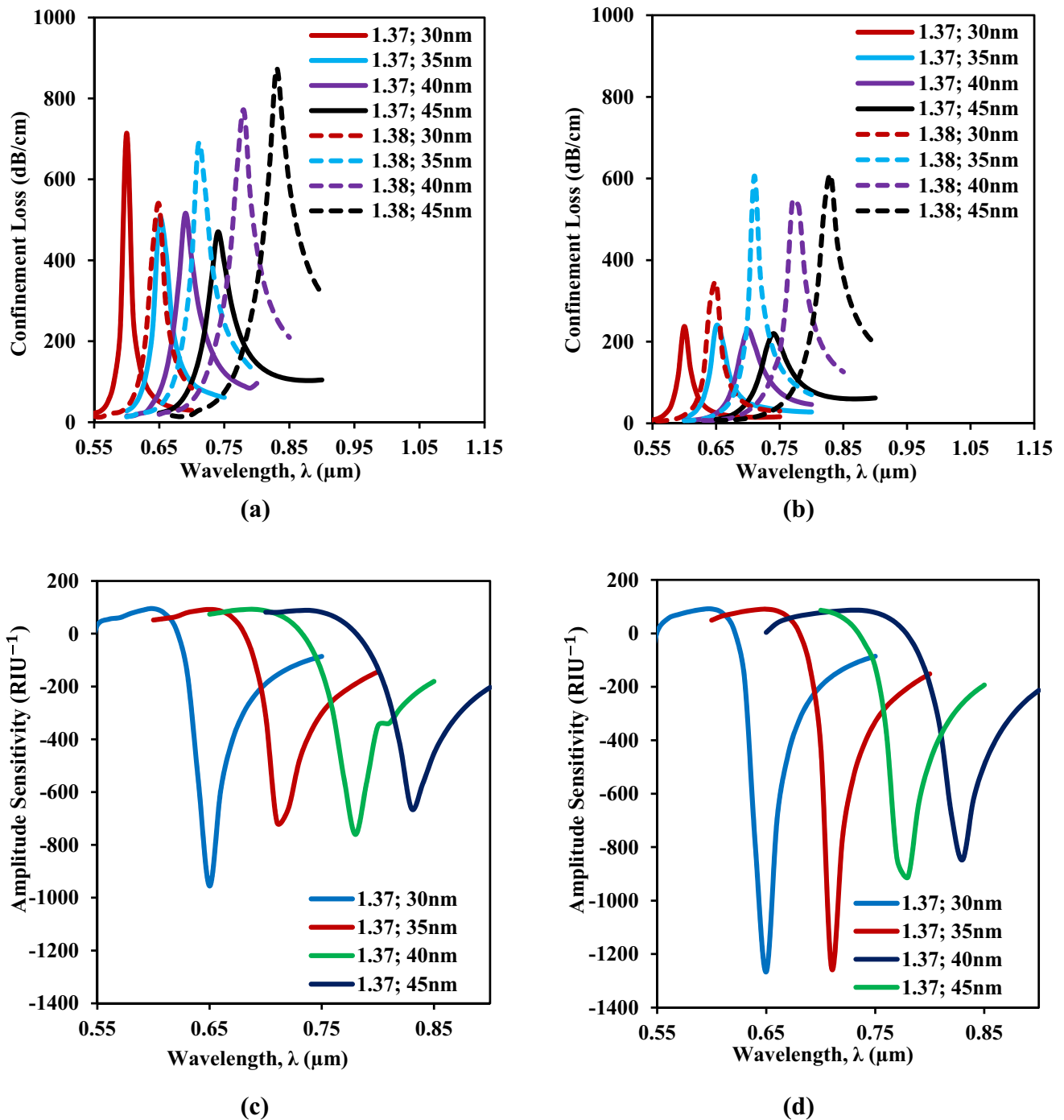
Fig. 4 Effect of variation of gold layer for the offered sensor on **a** confinement loss for *x*-polarized light, **b** confinement loss for *y*-polarized light, and **c** amplitude sensitivity for *x*-polarized light, and **d** amplitude sensitivity for *y*-polarized light

$$S_\lambda(\text{nm/RIU}) = \partial\lambda_p / \partial n_a \qquad (4)$$

where $\partial\lambda_p$ is the displacement between the resonance wavelength of two loss curve for two adjacent analytes and ∂n_a is the difference between two analytes. Figure 5a, b reflects the confinement loss with the gold thickness of 35 nm as a function of wavelength both for *x*- and

y-component of light. The variation of analyte refractive indices causes the change in the effective refractive index of SPP mode causing the shift in resonance wavelength of the loss spectrum. It is evident from the figure that the resonance wavelength of the loss spectrum shifts from longer to shorter wavelength with the increase in RI of the analyte as the real part of the effective refractive index of
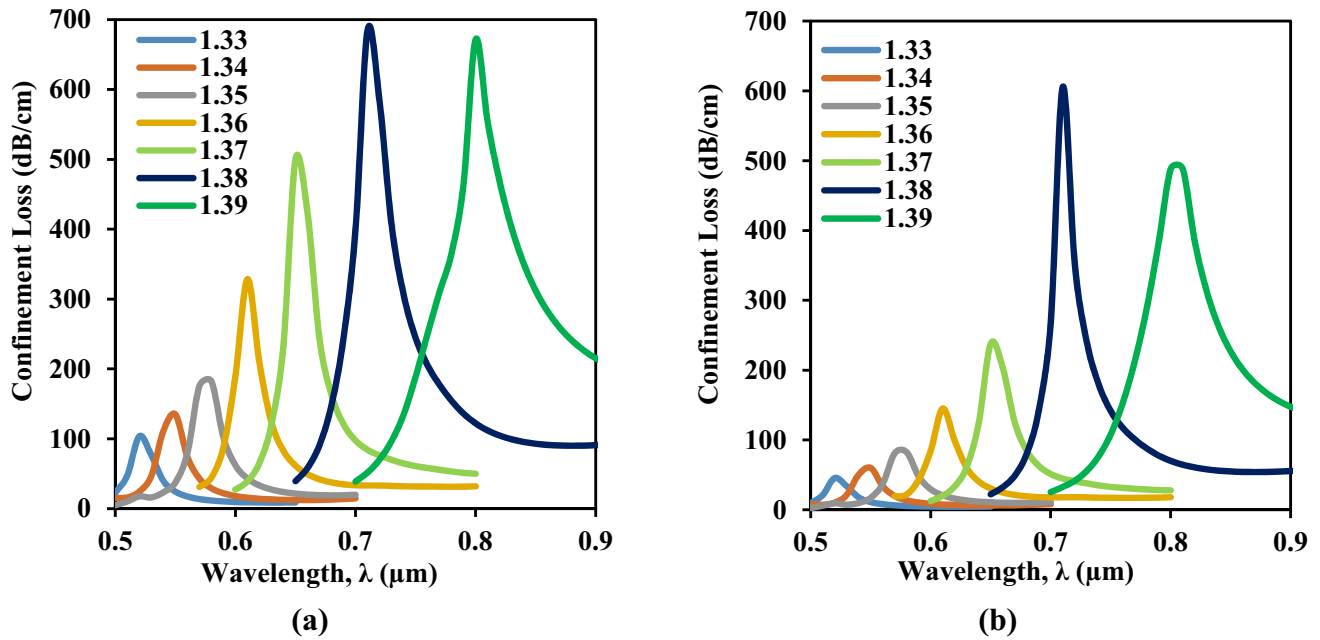
Fig. 5 Loss curves of the proposed sensor with optimized structure for **a** *x*-component of light and, **b** *y*-component of light for different analyte RI ranging from 1.33 to 1.39

SPP mode changes with the change of analyte RI. Examining the loss spectrum for analyte RI indices of 1.33, 1.34, 1.35, 1.36, 1.37, 1.38, and 1.39, it is observed that the resonance of loss curves is found at wavelength of 520 nm, 550 nm, 580 nm, 610 nm, 650 nm, 710 nm, and 810 nm, respectively, for two adjacent analyte RIs both for *x*- and *y*-component of light.

The peak of loss spectrum shifts 30 nm, 30 nm, 30 nm, 30 nm, 40 nm, 60 nm, and 100 nm for variation of analyte RI of 1.33–1.34, 1.34–1.35, 1.35–1.36, 1.36–1.37, 1.37–1.38, and 1.38–1.39, respectively. Using Eq. 4, the wavelength sensitivity of the sensor is calculated 3000 nm/RIU, 3000 nm/RIU, 3000 nm/RIU, 3000 nm/RIU, 4000 nm/RIU, 6000 nm/RIU, and 10,000 nm/RIU, respectively, for the variation of RIs ranging from 1.33 to 1.39. Hence, the maximum wavelength sensitivity of the sensor is measured 10,000 nm/RIU with an average value of 4571.429 nm/RIU.

3.2 Detection Accuracy, FOM, and Sensor Wavelength Resolution

Another important parameter, called detection accuracy of the sensor, is directly related to the sharpness of the loss curve. The detection accuracy of the sensor is determined by using the following equation [9].

$$D_{n_a} = 1/\text{FWHM} \tag{5}$$

where D_{n_a} is detection accuracy and FWHM is full width at half maxima of the loss curve of for analyte RI of n_a. From Fig. 5a, b it is observed that the values of FWHM for the corresponding analyte RI of 1.33, 1.34, 1.35, 1.36, 1.37, 1.38, and 1.39 are found 25, 30, 30, 26, 24, 39, and 67 nm for *x*-component and 25, 30, 31, 29, 32, 23, and 67 nm for *y*-component of light. The lower value of FWHM indicates the sharpness of the loss spectrum resulting in greater detection accuracy of the sensor. Another parameter related to FWHM is the figure of merit (FOM) of the sensor, which should be higher for better performance of the sensor. The FOM of the sensor is determined using the following equation [31].

$$\text{FOM(RIU}^{-1}) = \frac{S_\lambda}{\text{FWHM}} \tag{6}$$

Observing the values of FWHM and S_λ, it is found that the sensor gives a maximum value of FOM of 260.86 RIU^{-1} for the analyte RI of 1.37 for *y*-component of light. As well, wavelength resolution, considered a significant parameter for analysis of the performance of a sensor, is determined using the equation as follows [32].

$$R(\text{RIU}) = \frac{\partial \lambda_m \times \partial n_a}{\partial \lambda_p} \tag{7}$$

Considering the minimal spectral resolution of $\partial \lambda_m = 0.1$ nm and minimum analyte RI variation of $\partial n_a = 0.01$, the spectral resolution of the sensor is

Table 1 Performance comparison among the previously reported sensors and proposed one in this work

References	Description of structural design	Detection range	Operating wavelength (nm)	Wavelength sensitivity (nm/RIU)	Amplitude sensitivity (RIU^{-1})	Sensor resolution (RIU)	FOM (RIU^{-1})
Li et al. [16]	Externally gold-coated PCF sensor based on SPR	1.350–1.395	645–893	11,000	641	9.09×10^{-5}	–
Chakma et al. [17]	Gold-coated photonic crystal fiber biosensor based on SPR	1.340–1.370	620–710	9000	318	1.11×10^{-5}	–
Rifat et al. [18]	Solid core photonic crystal fiber RI sensor with external gold coating	1.330–1.370	615–745	4000	478	2.5×10^{-5}	–
Zhou et al. [19]	Ring-shaped externally coated PCF sensor	1.330–1.410	1310–1570	6900	132	–	–
Hasan et al. [20]	SPR photonic crystal fiber sensor with gold and niobium nanofilm layer	1.360–1.400	740–1000	8000	1560	8.64×10^{-5}	171.5
Paul et al. [21]	Dual-core structured SPR biosensor	1.330–1.410	600–980	11,500	636.5	8.7×10^{-6}	–
Akter et al. [22]	open channel-based PCF biosensor based on SPR	1.330–1.380	590–750	5000	396	2.0×10^{-5}	47
(This work)	PCF-based plasmonic microbiosensor: an external sensing approach	1.330–1.380	520–810	10,000	1250	1.0×10^{-5}	260.86

calculated as presented in Table 1, where the maximum value is tabulated as 1.0×10^{-5}. This value indicates that the raised sensor is capable of detecting a very small change in RI of the analyte of order 10^{-5}.

3.3 Amplitude Sensitivity

In addition to the phase detection method, another parameter based on amplitude interrogation of loss curve, called amplitude sensitivity, is used for exploring
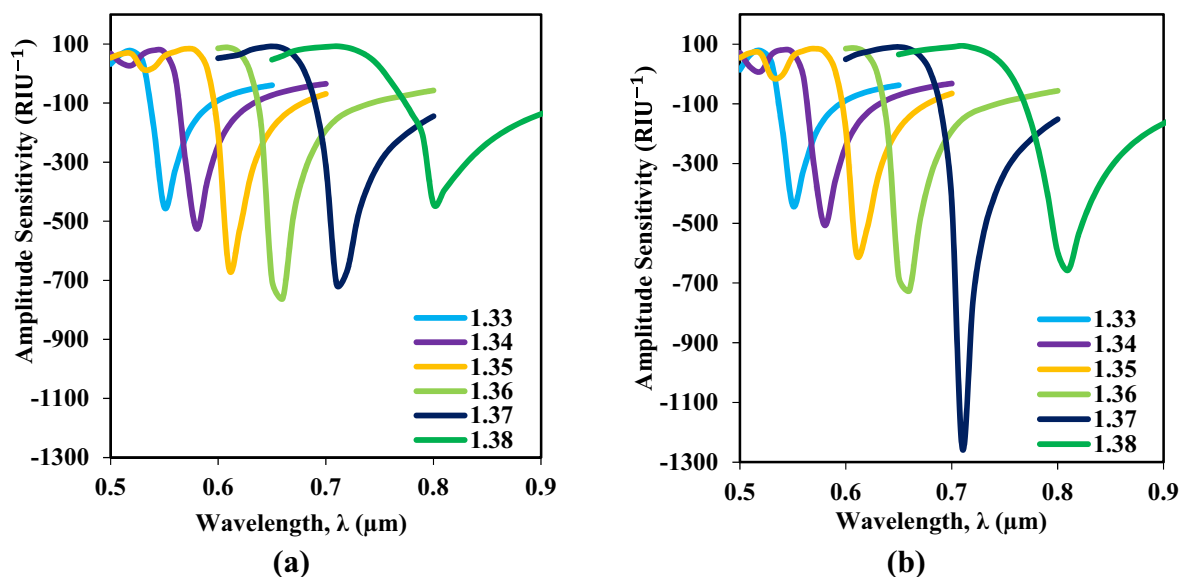

Fig. 6 Variation of amplitude sensitivity of the proposed sensor with varying analyte refractive index ranging from 1.33 to 1.38 both for **a** x-component and **b** y-component of light

the performance of the sensor. The amplitude sensitivity of the raised sensor is obtained using Eq. (3). Figure 6a, b represents the amplitude sensitivity of the raised sensor for analyte RI ranging from 1.33 to 1.38 with an interval of 0.01. It is seen that maximum amplitude sensitivity for x-component of light is observed at a wavelength of 650 nm for analyte RI of 1.36 and for y-component of light, it is at wavelength 710 nm for analyte RI of 1.37. It is found that the raised sensor confirms a high amplitude sensitivity of 810 RIU^{-1} and 1250 RIU^{-1} for x- and y-component of light, respectively, an indication of the promising performance of the proposed one. In the case of fabrication of fiber, the fiber may differ from its original structure and the structural parameter may be changed. So, the effect of variation of the structural parameter, e.g., pitch and diameter of air holes on amplitude sensitivity are also analyzed.

It is promising that higher accuracy is maintained during the fabrication process and the deviation is controlled within ± 1% of the designed structure [33]. For justification of the high amplitude sensitivity of the proposed structure, in case of variation of structural parameter due to the fabrication process, the performance is analyzed considering ± 1% tolerance of pitch variation. In this analysis, the diameter of the air holes is varied as a function of pitch. Figure 7a–d spectacles the response of the sensor for indicated pitch variation where Fig. 7a, b shows the loss spectrum variation and Fig. 7c, d shows the variation of amplitude sensitivity. It is noticed that for x-polarized light, the confinement loss increases with the escalation of pitch and resonance wavelength shifts to longer wavelength. On the other hand, confinement loss, and amplitude sensitivity for y-polarized light drop for both the case increasing and decreasing of pitch variation. While increasing the pitch, the distance between core to plasmonic material of the sensor increases, resulting in the less evanescent field to the interface resulting in less amplitude sensitivity whereas lessening of pitch also causes less path for the propagation of light between the neighboring air hole resulting less sensitivity. As well, the resonant wavelength shifts with the change of pitch, but it is very insignificant as shown in inset of Fig. 7c, d. It is observed that, due to variation of structure within the tolerable limit, minimum amplitude sensitivity of the sensor is calculate700 RIU^{-1} and 1050 RIU^{-1} for x- and y-polarized light, respectively, which indicates the good performance of the proposed structure.

3.4 Regression analysis

While analyzing the performance of the raised sensor, regression analysis is performed for determining the linearity property of the resonance wavelength concerning the variation of analyte refractive indices. The linearity

property promises a good sensor for further interpolation of resonant wavelength at some other value of analyte RI. Figure 8 represents a good linear fitting of the resonance wavelength which directs high accuracy of the raised sensor for the determination of analyte refractive indices. The liner line fitting of wavelength offers the regression equation as follows, while the linear regression value of the fitted line is $R^2 = 0.9465$.

$$\lambda_{resonance} = 4.3929 \times RI_{analyte} - 5.3429 \qquad (8)$$

Here, $\lambda_{resonance}$ and $RI_{analyte}$ indicates resonance wavelength and analyte refractive index of the sensor, respectively.

The following table shows the comparison among the proposed sensor in this work and the previously noted SPR sensors.

A generalized experimental setup for sensing the analyte is depicted in Fig. 9. The proposed mechanism includes a tunable optical source followed by a beam polarizer and optical spectrum analyzer (OSA) connected through optical fiber [34]. Mainly, the polarizer helps to select the one of two orthogonal (TE or TM) modes. The analyte, at the proposed sensor's outer surface, is controlled by a pump through the IN and OUT line. When light passes through the PCF sensor the interaction occurs with the plasmonic materials causing the propagation loss [35]. Then, simply using PCFs propagation loss measurement technique, the proposed sensor can be implemented to detect various analytes [26].

4 Conclusion

A highly sensitive PCF SPR sensor with an optimized gold layer, for the detection of biological and biochemical analytes, is proposed and characterized through numerical simulation. Different structural parameters, e.g., thickness of the gold sheet, diameter of the PCF air holes, and pitch, have been varied and examined to evaluate the characteristics of the sensor and improve the performance. The proposed sensor offers an enhanced performance characteristic with a maximum amplitude sensitivity of 810 RIU^{-1} and 1250 RIU^{-1} for x- and y-polarized light, respectively, at an optimized gold layer thickness of 35 nm. It should also be noted that the proposed sensor shows a maximum wavelength sensitivity of 10,000 nm/RIU with average wavelength sensitivity of 4571.429 nm/RIU. The sensor also shows a good wavelength resolution index of 1.0×10^{-5} RIU with highly linear regression characteristics with a value of $R^2 = 0.9465$. In addition, the sensor shows an excellent figure of merit (FOM) of the highest value of 260.86 RIU^{-1} validating its performance enhancements. Based on these auspicious
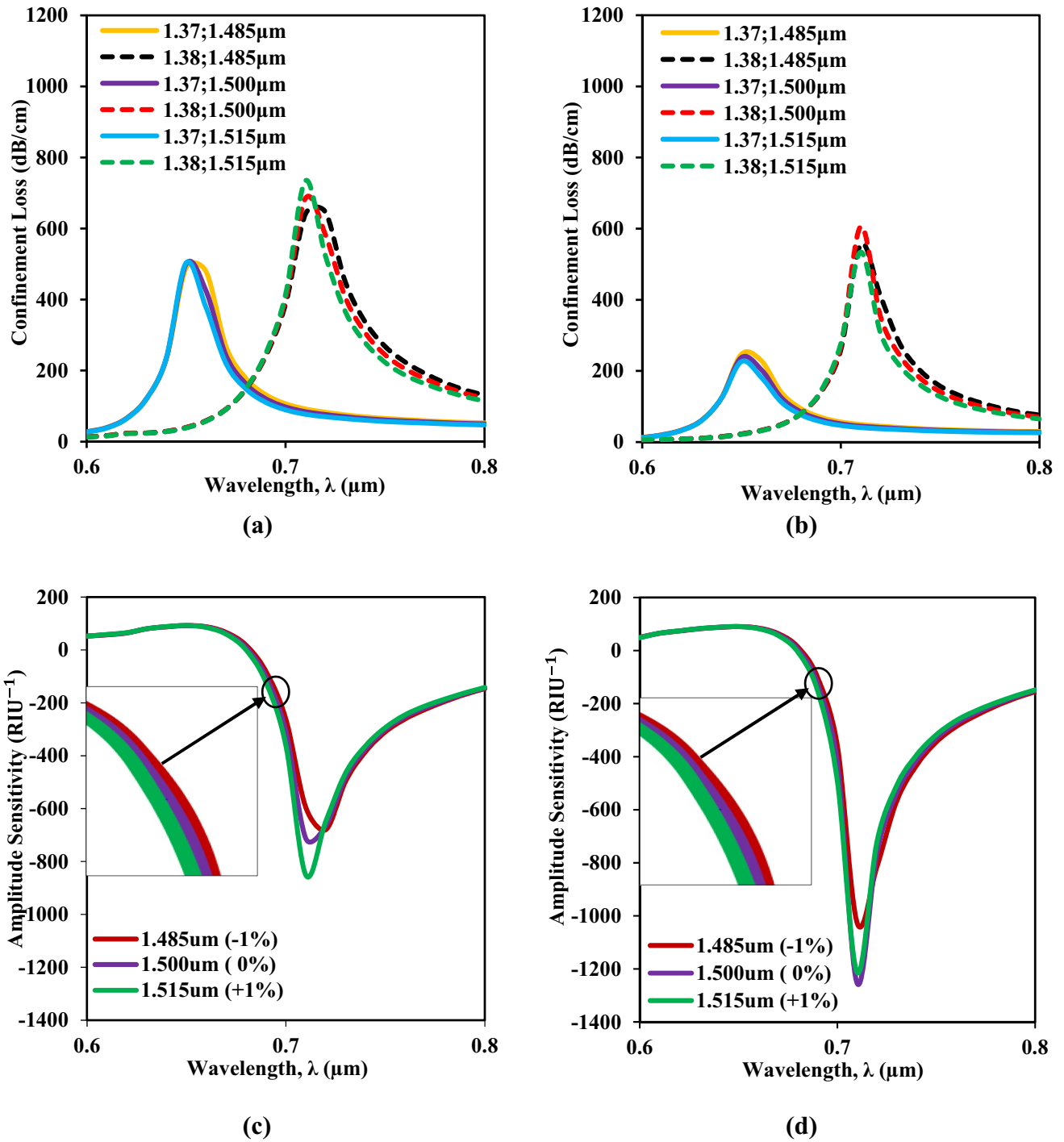
Fig. 7 Effect of variation of pitch (1.5 μm ± 1% of 1.5 μm) on **a** confinement loss for *x*-polarized light, **b** confinement loss for *y*-polarized light and **c** amplitude sensitivity for *x*-polarized light, **d** amplitude sensitivity for *y*-polarized light
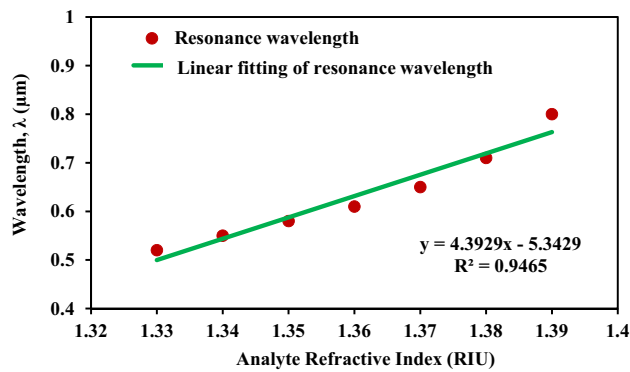
Fig. 8 Spectrum showing the linear fitting of resonance wavelength for the proposed sensor as a function of the analyte refractive index
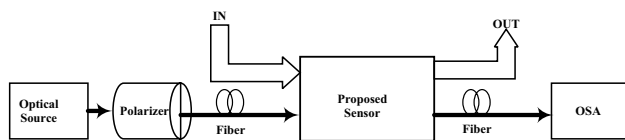

Fig. 9 Schematic experimental setup of the proposed sensor for detecting various analytes

performance attributes, the proposed sensor could be a promising one for myriad number applications for biochemical and biological liquid analyte detection.

Compliance with ethical standards

Conflict of interest The authors declare that they have no known competing financial interests or personal relationships that could have appeared to influence the work reported in this paper.

References

1. An G, Li S, Yan X, Yuan Z, Zhang X (2016) High-birefringence photonic crystal fiber polarization filter based on surface plasmon resonance. Appl Opt 55(6):1262–1266. https://doi.org/10.1364/AO.55.001262
2. Islam MS, Sultana J, Rifat AA, Ahmed R, Dinovitser A, Ng BW-H, Ebendorff-Heidepriem H, Abbott D (2018) Dual-polarized highly sensitive plasmonic sensor in the visible to near-IR spectrum. Opt Express 26(23):30347–30361. https://doi.org/10.1364/OE.26.030347
3. Wang F, Sun Z, Liu C, Sun T, Chu PK (2017) A highly sensitive dual-core photonic crystal fiber based on a surface plasmon resonance biosensor with silver-graphene layer. Plasmonics 12(6):1847–1853. https://doi.org/10.1007/s11468-016-0453-5
4. Zhang Y, Xia L, Zhou C, Yu X, Liu H, Liu D, Zhang Y (2011) Microstructured fiber based plasmonic index sensor with optimized accuracy and calibration relation in large dynamic range. Optics Communications 284(18):4161–4166. https://doi.org/10.1016/j.optcom.2011.04.053
5. Zhao Y, Deng Z-q, Li J (2014) Photonic crystal fiber based surface plasmon resonance chemical sensors. Sens Actuators B Chem 202:557–567. https://doi.org/10.1016/j.snb.2014.05.127
6. Rifat AA, Ahmed R, Yetisen AK, Butt H, Sabouri A, Mahdiraji GA, Yun SH, Adikan FM (2017) Photonic crystal fiber based plasmonic sensors. Sens Actuators B Chem 243:311–325. https://doi.org/10.1016/j.snb.2016.11.113
7. Ritchie RH (1957) Plasma losses by fast electrons in thin films. Phys Rev 106(5):874. https://doi.org/10.1103/PhysRev.106.874
8. Hassani A, Gauvreau B, Fehri MF, Kabashin A, Skorobogatiy M (2008) Photonic crystal fiber and waveguide-based surface plasmon resonance sensors for application in the visible and near-IR. Electromagnetics 28(3):198–213. https://doi.org/10.1080/02726340801921627
9. Rifat AA, Mahdiraji GA, Sua YM, Ahmed R, Shee Y, Adikan FM (2016) Highly sensitive multi-core flat fiber surface plasmon resonance refractive index sensor. Opt Express 24(3):2485–2495. https://doi.org/10.1364/OE.24.002485
10. Aoni RA, Ahmed R, Alam MM, Razzak S (2013) Optimum design of a nearly zero ultra-flattened dispersion with lower confinement loss photonic crystal fibers for communication systems. Int J Sci Eng Res 4:1–4
11. Haider F, Aoni RA, Ahmed R, Islam MS, Miroshnichenko AE (2018) Propagation controlled photonic crystal fiber-based plasmonic sensor via scaled-down approach. IEEE Sens J 19(3):962–969. https://doi.org/10.1109/JSEN.2018.2880161
12. Gandhi MA, Babu PR, Senthilnathan K, Li Q (2018) High sensitivity photonic crystal fiber-based refractive index microbiosensor. Optical Fiber Technology 46:88–94. https://doi.org/10.1016/j.yofte.2018.09.016
13. Akowuah E, Gorman T, Ademgil H, Haxha SA (2012) Highly sensitive photonic crystal fibre (PCF) surface plasmon resonance (SPR) sensor based on a bimetallic structure of gold and silver. In: 2012 IEEE 4th International conference on adaptive science & technology (ICAST), 2012. IEEE, pp 121–125. https://doi.org/10.1109/ICASTech.2012.6381078
14. Meshginqalam B, Barvestani J (2018) Performance enhancement of SPR biosensor based on phosphorene and transition metal dichalcogenides for sensing DNA hybridization. IEEE Sens J 18(18):7537–7543. https://doi.org/10.1109/JSEN.2018.2861829
15. Rahman MS, Anower MS, Hasan MR, Hossain MB, Haque MI (2017) Design and numerical analysis of highly sensitive Au-MoS_2-graphene based hybrid surface plasmon resonance biosensor. Optics Communications 396:36–43. https://doi.org/10.1016/j.optcom.2017.03.035
16. Li X, Li S, Yan X, Sun D, Liu Z, Cheng T (2018) High sensitivity photonic crystal fiber refractive index sensor with gold coated externally based on surface plasmon resonance. Micromachines 9(12):640. https://doi.org/10.3390/mi9120640
17. Chakma S, Khalek MA, Paul BK, Ahmed K, Hasan MR, Bahar AN (2018) Gold-coated photonic crystal fiber biosensor based on surface plasmon resonance: design and analysis. Sensing and bio-sensing Research 18:7–12. https://doi.org/10.1016/j.sbsr.2018.02.003
18. Rifat AA, Hasan MR, Ahmed R, Butt H (2017) Photonic crystal fiber-based plasmonic biosensor with external sensing approach. J Nanophotonics 12(1):012503. https://doi.org/10.1117/1.JNP.12.012503
19. Zhou X, Cheng T, Li S, Suzuki T, Ohishi Y (2018) Practical sensing approach based on surface plasmon resonance in a photonic crystal fiber. OSA Continuum 1(4):1332–1340. https://doi.org/10.1364/OSAC.1.001332
20. Hasan MR, Akter S, Ahmed K, Abbott D (2017) Plasmonic refractive index sensor employing niobium nanofilm on photonic

crystal fiber. IEEE Photonics Technol Lett 30(4):315–318. https://doi.org/10.1109/LPT.2017.2786475

21. Paul AK, Sarkar AK, Khaleque A (2019) Dual-core photonic crystal fiber plasmonic refractive index sensor: a numerical analysis. Photonic Sensors 9(2):151–161. https://doi.org/10.1007/s13320-018-0524-7

22. Akter S, Razzak SA (2019) Highly sensitive open-channels based plasmonic biosensor in visible to near-infrared wavelength. Results Phys 13:102328. https://doi.org/10.1016/j.rinp.2019.102328

23. Rifat AA, Haider F, Ahmed R, Mahdiraji GA, Adikan FM, Miroshnichenko AE (2018) Highly sensitive selectively coated photonic crystal fiber-based plasmonic sensor. Opt Lett 43(4):891–894. https://doi.org/10.1364/OL.43.000891

24. Hu DJJ, Ho HP (2017) Recent advances in plasmonic photonic crystal fibers: design, fabrication and applications. Adv Opt Photonics 9(2):257–314. https://doi.org/10.1364/AOP.9.000257

25. Haque E, Mahmuda S, Hossain MA, Hai NH, Namihira Y, Ahmed F (2019) Highly sensitive dual-core PCF based plasmonic refractive index sensor for low refractive index detection. IEEE Photonics J 11(5):1–9. https://doi.org/10.1109/JPHOT.2019.2931713

26. Haider F, Aoni RA, Ahmed R, Miroshnichenko AE (2018) Highly amplitude-sensitive photonic-crystal-fiber-based plasmonic sensor. JOSA B 35(11):2816–2821. https://doi.org/10.1364/JOSAB.35.002816

27. Akowuah EK, Gorman T, Ademgil H, Haxha S, Robinson GK, Oliver JV (2012) Numerical analysis of a photonic crystal fiber for biosensing applications. IEEE J Quantum Electron 48(11):1403–1410. https://doi.org/10.1109/JQE.2012.2213803

28. Liu C, Yang L, Su W, Wang F, Sun T, Liu Q, Mu H, Chu PK (2017) Numerical analysis of a photonic crystal fiber based on a surface plasmon resonance sensor with an annular analyte channel. Optics Communications 382:162–166. https://doi.org/10.1016/j.optcom.2016.07.031

29. Gao D, Guan C, Wen Y, Zhong X, Yuan L (2014) Multi-hole fiber based surface plasmon resonance sensor operated at near-infrared wavelengths. Opt Commun 313:94–98. https://doi.org/10.1016/j.optcom.2013.10.015

30. Gandhi MA, Senthilnathan K, Babu PR, Li Q (2019) Visible to near infrared highly sensitive microbiosensor based on surface plasmon polariton with external sensing approach. Results Phys 15:102590. https://doi.org/10.1016/j.rinp.2019.102590

31. Fan Z, Li S, Liu Q, An G, Chen H, Li J, Chao D, Li H, Zi J, Tian W (2015) High sensitivity of refractive index sensor based on analyte-filled photonic crystal fiber with surface plasmon resonance. IEEE Photonics J 7(3):1–9. https://doi.org/10.1109/JPHOT.2015.2432079

32. Gangwar RK, Singh VK (2017) Highly sensitive surface plasmon resonance based D-shaped photonic crystal fiber refractive index sensor. Plasmonics 12(5):1367–1372. https://doi.org/10.1007/s11468-016-0395-y

33. Reeves WH, Knight J, Russell PSJ, Roberts P (2002) Demonstration of ultra-flattened dispersion in photonic crystal fibers. Opt Express 10(14):609–613. https://doi.org/10.1364/OE.10.000609

34. Mahfuz MA, Hossain M, Haque E, Hai NH, Namihira Y, Ahmed F (2019) A bimetallic-coated, low propagation loss, photonic crystal fiber based plasmonic refractive index sensor. Sensors 19(17):3794. https://doi.org/10.3390/s19173794

35. Mollah MA, Islam SR, Yousufali M, Abdulrazak LF, Hossain MB, Amiri I (2020) Plasmonic temperature sensor using D-shaped photonic crystal fiber. Results Phys 16:102966. https://doi.org/10.1016/j.rinp.2020.102966